



Article

Effect of TiO₂ Film Thickness on the Stability of Au₉ Clusters with a CrO_x Layer

Abdulrahman S. Alotabi ^{1,2,3} , Yanting Yin ^{1,3}, Ahmad Redaa ^{4,5} , Siriluck Tesana ^{6,7}, Gregory F. Metha ^{8,*} and Gunther G. Andersson ^{1,3,*}

- ¹ Flinders Institute for Nanoscale Science and Technology, Flinders University, Adelaide, SA 5042, Australia
² Department of Physics, Faculty of Science and Arts in Baljurashi, Albaha University, Baljurashi 65655, Saudi Arabia
³ Flinders Microscopy and Microanalysis, College of Science and Engineering, Flinders University, Adelaide, SA 5042, Australia
⁴ Department of Earth Sciences, University of Adelaide, Adelaide, SA 5005, Australia
⁵ Faculty of Earth Sciences, King Abdulaziz University, Jeddah 21589, Saudi Arabia
⁶ The MacDiarmid Institute for Advanced Materials and Nanotechnology, School of Physical and Chemical Sciences, University of Canterbury, Christchurch 8041, New Zealand
⁷ National Isotope Centre, GNS Science, Lower Hutt 5010, New Zealand
⁸ Department of Chemistry, University of Adelaide, Adelaide, SA 5005, Australia
* Correspondence: greg.metha@adelaide.edu.au (G.F.M.); gunther.andersson@flinders.edu.au (G.G.A.)
† Current address: Physical Sciences Building, (2111) GPO Box 2100, Adelaide, SA 5001, Australia.

Abstract: Radio frequency (RF) magnetron sputtering allows the fabrication of TiO₂ films with high purity, reliable control of film thickness, and uniform morphology. In the present study, the change in surface roughness upon heating two different thicknesses of RF sputter-deposited TiO₂ films was investigated. As a measure of the process of the change in surface morphology, chemically -synthesised phosphine-protected Au₉ clusters covered by a photodeposited CrO_x layer were used as a probe. Subsequent to the deposition of the Au₉ clusters and the CrO_x layer, samples were heated to 200 °C to remove the triphenylphosphine ligands from the Au₉ cluster. After heating, the thick TiO₂ film was found to be mobile, in contrast to the thin TiO₂ film. The influence of the mobility of the TiO₂ films on the Au₉ clusters was investigated with X-ray photoelectron spectroscopy. It was found that the high mobility of the thick TiO₂ film after heating leads to a significant agglomeration of the Au₉ clusters, even when protected by the CrO_x layer. The thin TiO₂ film has a much lower mobility when being heated, resulting in only minor agglomeration of the Au₉ clusters covered with the CrO_x layer.

Keywords: RF magnetron sputtering; TiO₂ film; morphology; triphenylphosphine; Au₉; gold clusters; photodeposition; CrO_x; Cr(OH)₃; Cr₂O₃ layer



Citation: Alotabi, A.S.; Yin, Y.; Redaa, A.; Tesana, S.; Metha, G.F.; Andersson, G.G. Effect of TiO₂ Film Thickness on the Stability of Au₉ Clusters with a CrO_x Layer. *Nanomaterials* **2022**, *12*, 3218. <https://doi.org/10.3390/nano12183218>

Academic Editor: Orion Ciftja

Received: 17 August 2022

Accepted: 9 September 2022

Published: 16 September 2022

Publisher's Note: MDPI stays neutral with regard to jurisdictional claims in published maps and institutional affiliations.



Copyright: © 2022 by the authors. Licensee MDPI, Basel, Switzerland. This article is an open access article distributed under the terms and conditions of the Creative Commons Attribution (CC BY) license (<https://creativecommons.org/licenses/by/4.0/>).

1. Introduction

Titanium dioxide (TiO₂) is a semiconductor widely used for a large range of photocatalytic applications and is also an ideal model system for various types of studies [1,2]. There are various techniques to prepare TiO₂ films, such as sol-gel [3], evaporation [4], chemical vapour deposition [5], atomic layer deposition [6] and radio frequency (RF) magnetron sputtering [7]. Each of these methods has advantages and disadvantages in regard to fabrication costs, uniformity of the film morphology, thermal stability, purity and preparation time. Therefore, the best method of choice for TiO₂ film preparation depends on which application the film will be used in.

Amongst the above-named methods, RF magnetron sputtering is known to produce high-purity TiO₂ films with uniform thickness, ease of use and strong film adhesion to the substrate [8]. The properties of these films are significantly impacted by the sputtering

conditions, such as RF power, gas pressure, substrate type, substrate temperature and target-to-substrate distance [9–14]. For instance, it has been reported that control of TiO₂ film thickness is possible by modulating the deposition time and the gas sputtering pressure [15].

TiO₂ films prepared with the RF magnetron sputtering method can be amorphous or have a rutile, anatase, or brookite crystal structure. It is well known that the physical properties of TiO₂ films depend highly on the post-deposition treatment, including heat treatment conditions [16–18]. Çörekçi et al. reported that a correlation between heating treatment and surface morphology with different TiO₂ film thicknesses. It was observed that an increase in surface roughness and grain sizes occurred during heating depending on TiO₂ film thicknesses, which also increased with film thickness. This is because increasing temperatures transform TiO₂ from amorphous to anatase and then to rutile [17], and these phase transitions affect the surface morphology of the TiO₂ film, which includes the roughness and crystallinity of the surface [19].

The aim of this study is to investigate the influence of heat treatment on the surface morphology of RF sputter-deposited TiO₂ films with two different thicknesses, and the effect this has on size-specific Au clusters deposited on the surface. TiO₂ films have attracted interest as substrates for investigating the role of Au clusters as cocatalysts in photocatalysis [20,21]. In these studies, TiO₂ films had been heated as part of the sample preparation procedure. The change in morphology, including surface mobility, upon heating, can lead to agglomeration of the Au clusters. Understanding the change in surface morphology upon heating, thus, is important when using TiO₂ as a substrate for investigating the cocatalyst properties. In the present work, phosphine-protected Au₉ clusters covered by a photodeposited CrO_x layer were used as probes for the TiO₂ mobility during the change of morphology upon heating. Scanning electron microscopy (SEM), X-ray diffraction (XRD), laser scanning confocal microscope (LSCM) and X-ray photoelectron spectroscopy (XPS), have been applied to characterise the thickness, crystal structure, surface morphology and chemical composition and size of the Au cluster. The importance of the present work is to show that morphology changes in RF sputter-deposited TiO₂ depend on the thickness of the TiO₂ layer, and that Au₉ clusters can be used to probe morphology changes in the surface.

2. Experimental Methods and Techniques

2.1. Material and Sample Preparation

2.1.1. Preparation of TiO₂ Films

The RF magnetron sputtering method was used to prepare TiO₂ films on a silicon wafer under high vacuum conditions (HHV/Edwards TF500 sputter coater) [22]. Before the deposition, the silicon wafer was cleaned with ethanol and acetone and then dried in a stream of dry nitrogen. The TiO₂ film was deposited onto a p-type silicon wafer substrate by sputtering a 99.9% pure TiO₂ ceramic target with 500 W sputtering power using Ar⁺ (flow rate of 5 sccm) for 50 min. The sputter coating chamber was held under vacuum at 2×10^{-5} mbar. This process resulted in TiO₂ films formed on the silicon wafer with a native oxide layer of TiO₂.

TiO₂ films with two different thickness were fabricated applying the above-described procedure. The TiO₂ films had different colours based on light interference [23]: a TiO₂/Si wafer with a purple colour and a TiO₂/Si wafer with a gold-like colour (see Figure S1). The difference in colour of the films is related to the difference in light interference patterns within the films due to their difference in film thickness [24]. The thickness of TiO₂P is ~400 nm, while TiO₂G is ~1100 nm (*vide infra*). The TiO₂ wafers were cut into 1 cm × 1 cm pieces and used without further treatment. The two TiO₂ wafers are hereafter referred to as (i) TiO₂P and (ii) TiO₂G.

2.1.2. Deposition of Au₉ Clusters

The deposition procedure of Au₉(PPh₃)₈(NO₃)₃ (Au₉) was identical for both the TiO₂P and TiO₂G samples. Phosphine-protected Au₉ clusters were synthesised as reported

previously [25]. A UV-Vis spectrum of the Au₉ cluster is shown in Figure S2. The TiO₂ films were immersed in Au₉ methanol solutions (2 mL) for 30 min at concentrations of 0.006, 0.06 and 0.6 mM. The TiO₂ samples were rinsed by quickly dipping them into pure methanol and then dried in a stream of dry nitrogen. These samples are hereafter referred to as (i) TiO₂P-Au₉ and (ii) TiO₂G-Au₉.

2.1.3. Photodeposition of CrO_x Layer

Photodeposition of the CrO_x layer was the same for both TiO₂-Au₉ samples (TiO₂P-Au₉ and TiO₂G-Au₉). A 0.5 mM potassium chromate solution was prepared by dissolving K₂CrO₄ (≥99%, Sigma-Aldrich) in deionised water. The TiO₂-Au₉ samples were immersed into the K₂CrO₄ solution (1 mL) and irradiated for 1 h using a UV LED (Vishay, VLMU3510-365-130) with ~1 cm between the sample and the irradiation source. The UV LED had a radiant power of 690 mW at 365 nm wavelength. After photodeposition, the samples were washed by dipping them into deionised water and dried in a stream of dry nitrogen [26]. These samples are hereafter referred to as (i) TiO₂P-Au₉-CrO_x and (ii) TiO₂G-Au₉-CrO_x.

2.1.4. Heat Treatment

To remove the phosphine ligands from Au₉ clusters, all samples were treated with heating at 200 °C for 10 min under ultra-high vacuum (1×10^{-8} mbar) in the XPS chamber.

2.2. Characterization Methods

2.2.1. Scanning Electron Microscopy and Energy Dispersive X-ray Spectroscopy (SEM-EDAX)

The thickness of TiO₂ films (TiO₂P and TiO₂G) was determined by combining SEM imaging and SEM-EDAX (FEI Inspect F50 microscope) scans on cross-sections of the TiO₂ samples. Cross-sectional images were recorded at a magnification of up to 100 k with 15 keV electron energy.

2.2.2. X-ray Diffraction (XRD)

The crystal and phase structure of the TiO₂ films (TiO₂P and TiO₂G) before and after heating were analysed using XRD. A Bruker D8 Advance apparatus was used to record the XRD patterns with an irradiation source of Co-Kα ($\lambda = 1.789$ Å) operating at 35 kV and 28 mA.

2.2.3. Laser Scanning Confocal Microscope (LSCM)

The surface morphology of TiO₂ films (TiO₂P and TiO₂G) was measured using a LSCM (Olympus LEXT OLS5000-SAF 3D LSCM) with 100x/0.80NA and 50x/0.60NA LEXT objective lenses. The Olympus Data Analysis software was used to calculate the arithmetic mean deviation (Ra) and root mean square deviation (Rq) values.

2.2.4. X-ray Photoelectron Spectroscopy (XPS)

XPS analysis was performed using an X-ray source with Mg Kα line ($h\nu = 1253.6$ eV). A detailed description of the equipment has been given previously [27]. Survey spectrum scans were performed with a pass energy of 40 eV using a SPECS PHOIBOS-HSA 3500 hemispherical analyser. High-resolution XPS spectra were recorded for C, O, P, Si, Ti, Cr and Au with a pass energy of 10 eV. All XPS binding energy scales were normalised using the C 1s peak at 285 eV. The peaks were fitted to calculate relative intensities considering atomic sensitivity factors. XPS was recorded immediately after sample preparation and heating, thus, reducing the number of atmospheric exposures.

3. Results and Discussion

3.1. Influence of the Thickness of the TiO₂ Films

The influence of the thickness of the RF sputter-deposited TiO₂ on the change in film morphology upon heating is investigated. First, we will determine the thickness of the TiO₂ films for TiO₂P and TiO₂G and describe the crystallinity and morphology of both samples before and after heating. Then, the XPS results will be reported for both TiO₂P and

TiO₂G. Subsequently, the agglomeration of Au₉ clusters beneath a Cr₂O₃ overlayer upon heating of the two films is determined and discussed.

3.2. Determination of the TiO₂ Film Thickness

Figure 1 shows cross-section SEM images of TiO₂P and TiO₂G with line measurements of the thickness of the TiO₂ films. These SEM images clearly show that the thickness of the film for the TiO₂P and TiO₂G samples is ~400 nm and ~1100 nm, respectively; the film thickness of TiO₂G is more than two times greater than for TiO₂P. To confirm the film thickness, EDAX was further processed at the same image spots as SEM. Cross-section SEM-EDAX elemental maps of Ti, O and Si of TiO₂P and TiO₂G are shown in Figure S3. The EDAX elemental maps confirm that the thickness of the TiO₂ film for TiO₂G is larger than for TiO₂P.

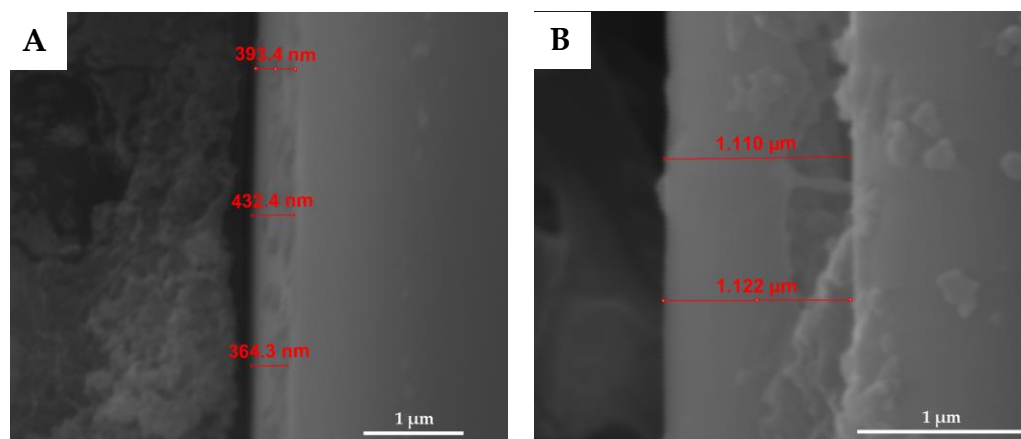


Figure 1. Cross-section SEM images of the (A) TiO₂P [28] and (B) TiO₂G layer.

3.3. Crystal Structure of the TiO₂P and TiO₂G before and after Heating

To assess the crystal structure of the TiO₂ film for TiO₂P and TiO₂G, XRD was conducted (Figure 2). There are no observable anatase, rutile or brookite crystal phase peaks [29], indicating that the films have an amorphous crystal structure. The crystallographic state of the TiO₂ is known to be transformed upon heating. The XRD patterns of TiO₂ films (TiO₂P and TiO₂G) after heating at 200 °C for 10 min are shown in Figure 2. Both spectra show an anatase peak at 29.8°, which confirms that the crystal structure of TiO₂P and TiO₂G has changed to the anatase phase after heating. The intensity of the anatase diffraction peak for TiO₂G is more than two times higher than for TiO₂P, which is due to the difference in the total amount of TiO₂ in each film. The TiO₂G layer is more than two times thicker than TiO₂P, so we also expect that there is more than twice as much anatase in the TiO₂G film. Thus, the percentage change in crystal structure in the films is comparable. The formation of the anatase phase strongly suggests the TiO₂ film could be mobile during the heating process, which could influence the morphology of the TiO₂ films, as will be discussed below.

3.4. Morphology of the TiO₂P and TiO₂G Layer before and after Heating

LSCM was conducted on both TiO₂ films before and after heating to compare their morphology. Figure 3 shows the surface morphology of TiO₂P and TiO₂G before and after heating over an area of 16 × 16 μm and the determined Ra and Rq values. The 3D profiles of the same spots are displayed in Figure S4. Before heating, the Ra (and Rq) values of the TiO₂P and TiO₂G are 0.6 nm (0.8 nm) and 1.0 nm (1.3 nm), respectively. However, after heating, the values become 1.0 nm (1.2 nm) and 12.7 nm (14.7 nm), respectively. The change in Ra (and Rq) for TiO₂P is small after heating, especially in comparison to TiO₂G, which is 12 times higher after heating. The Ra (and Rq) values were also calculated over a much larger area of 595 × 595 μm and show a similar change (Figure S5). The change in the Ra

(and R_q) values indicates that both the TiO_2P and TiO_2G increase in surface roughness after heating. The XRD results show that the TiO_2G and TiO_2P have the same fraction of anatase after heating, so the total amount of anatase in TiO_2G is larger compared to TiO_2P (vide supra). Çörekçi et al. noted a similar finding in their study of different thicknesses of TiO_2 films heated at different temperatures [19]. The authors reported that the surface roughness of the thicker TiO_2 film (300 nm) increased more compared to thinner films (220 and 260 nm) upon heating. In our study, a large change in the surface roughness was observed clearly with the thicker film (more than two times thicker) by a factor of six. Çörekçi et al. assumed that the increase in surface roughness was due to increases in the grain sizes with increasing film thickness and the recrystallization in the TiO_2 films during heating. A number of studies have reported comparable findings that the surface morphology of the TiO_2 films changes upon heating [17,30]. Thus, we conclude that the thicker TiO_2G film is more mobile during heating in comparison to the thinner film in the TiO_2P sample.

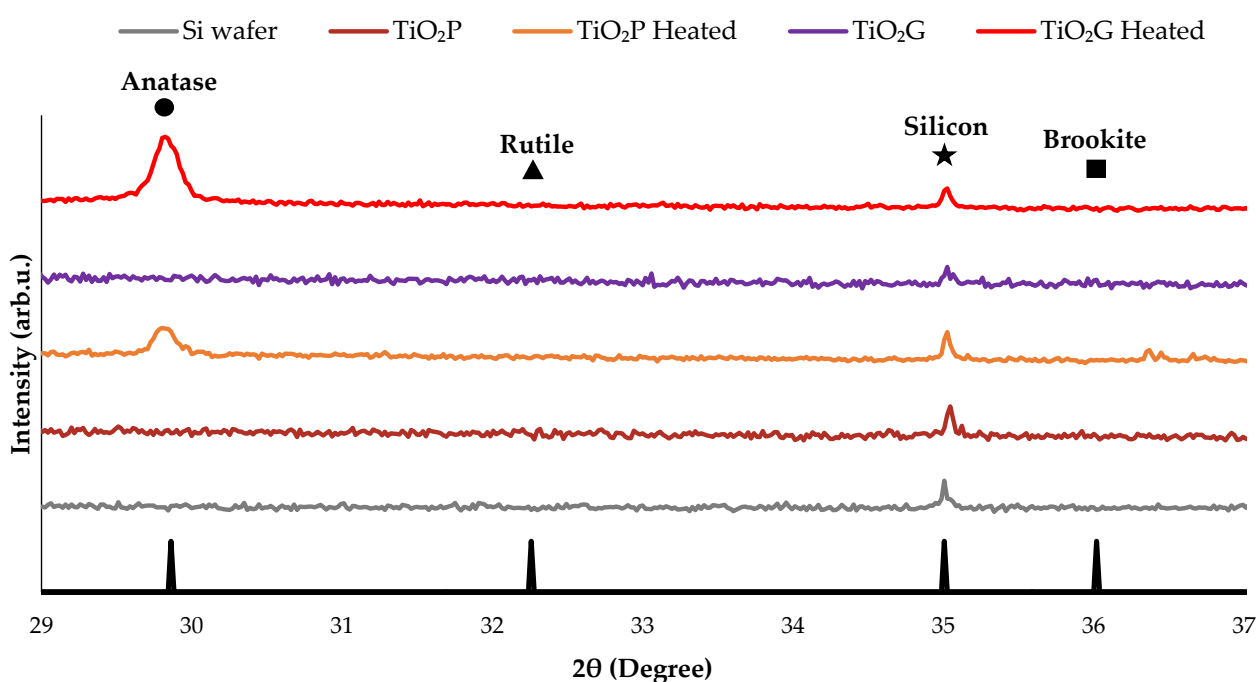


Figure 2. XRD patterns of the Si wafer, TiO_2P and TiO_2P after heating, TiO_2G and TiO_2G after heating to 200 °C. The positions of the diffraction peaks for anatase, rutile and brookite, as well as Si, are indicated using the standard XRD patterns (anatase PDF 01-075-1537, rutile PDF 01-071-4809, brookite PDF 04-007-0758 and Si PDF 00-013-0542).

3.5. Au_9 Clusters on TiO_2P and TiO_2G ; a Probe for Mobility during Heating

In order to provide insight into the mobility of the TiO_2 during the recrystallisation process, Au_9 clusters were deposited onto the TiO_2 films and analysed with XPS. XPS was used to investigate the size of phosphine-protected Au_9 clusters deposited onto TiO_2P and TiO_2G . In addition, the effect of the CrO_x overlayer on the Au_9 clusters was investigated, also with XPS. Figures 4 and 5 show the peak positions and relative intensities of $Au 4f_{7/2}$ peaks in the XP spectra of three different concentrations (0.006, 0.06 and 0.6 mM) of TiO_2P-Au_9 , TiO_2G-Au_9 , $TiO_2P-Au_9-CrO_x$ and $TiO_2G-Au_9-CrO_x$ before and after heating. Tables S1 and S2 show a summary of all the $Au 4f_{7/2}$ peak positions and full-width-half-maximum (FWHM). Note that all the $Au 4f$ spectra for both substrates (TiO_2P and TiO_2G) are shown in Figures S6 and S7. The TiO_2P XPS results will be first presented, followed by the TiO_2G results.

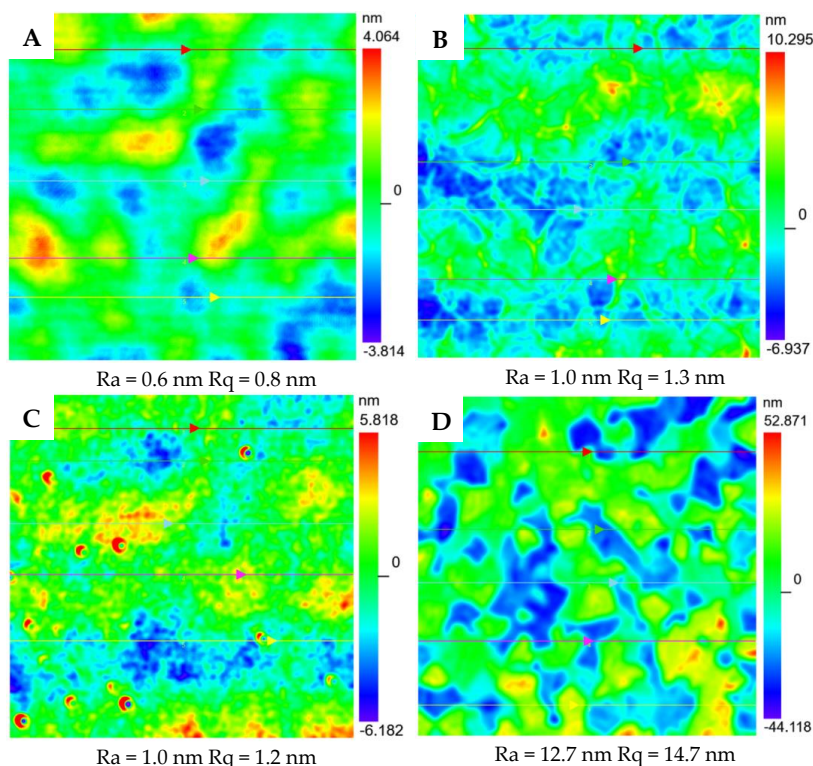


Figure 3. Surface morphology with the Ra and Rq values of (A) TiO₂P before heating and (B) TiO₂P after heating, (C) TiO₂G before heating and (D) TiO₂G after heating (area 16 × 16 μm). Note that the scale bars are different.

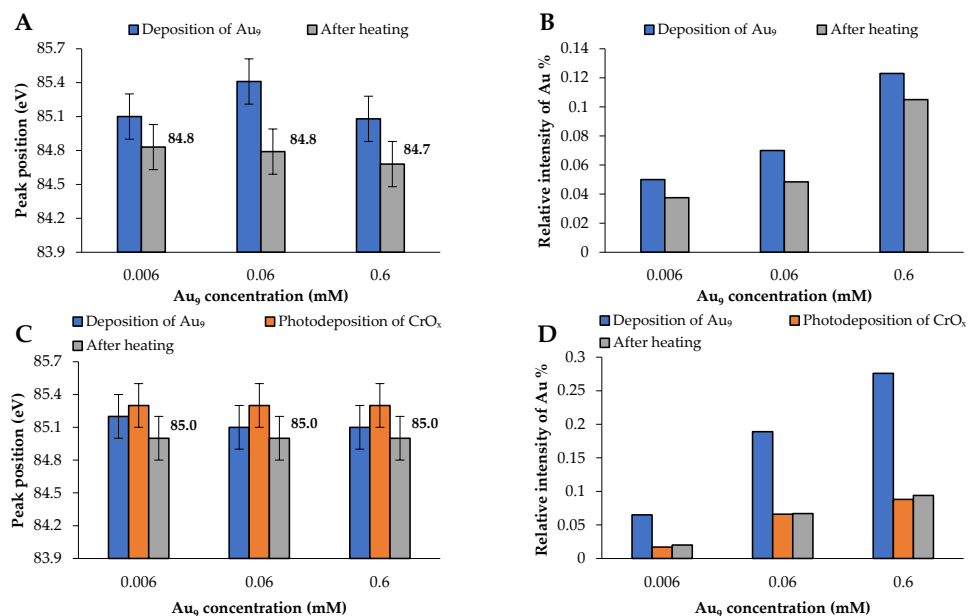


Figure 4. XPS results of TiO₂P-Au₉ for three different Au₉ concentrations: (A) position of Au 4f_{7/2} and (B) relative intensity of Au before and after heating. TiO₂P-Au₉-CrO_x (C) position of Au 4f_{7/2} and (D) relative intensity of Au before and after photodeposition of the CrO_x layer and after heating. Note that the vertical scales of (B,D) are different and that the samples in (A,C) are different but are prepared in the same manner.

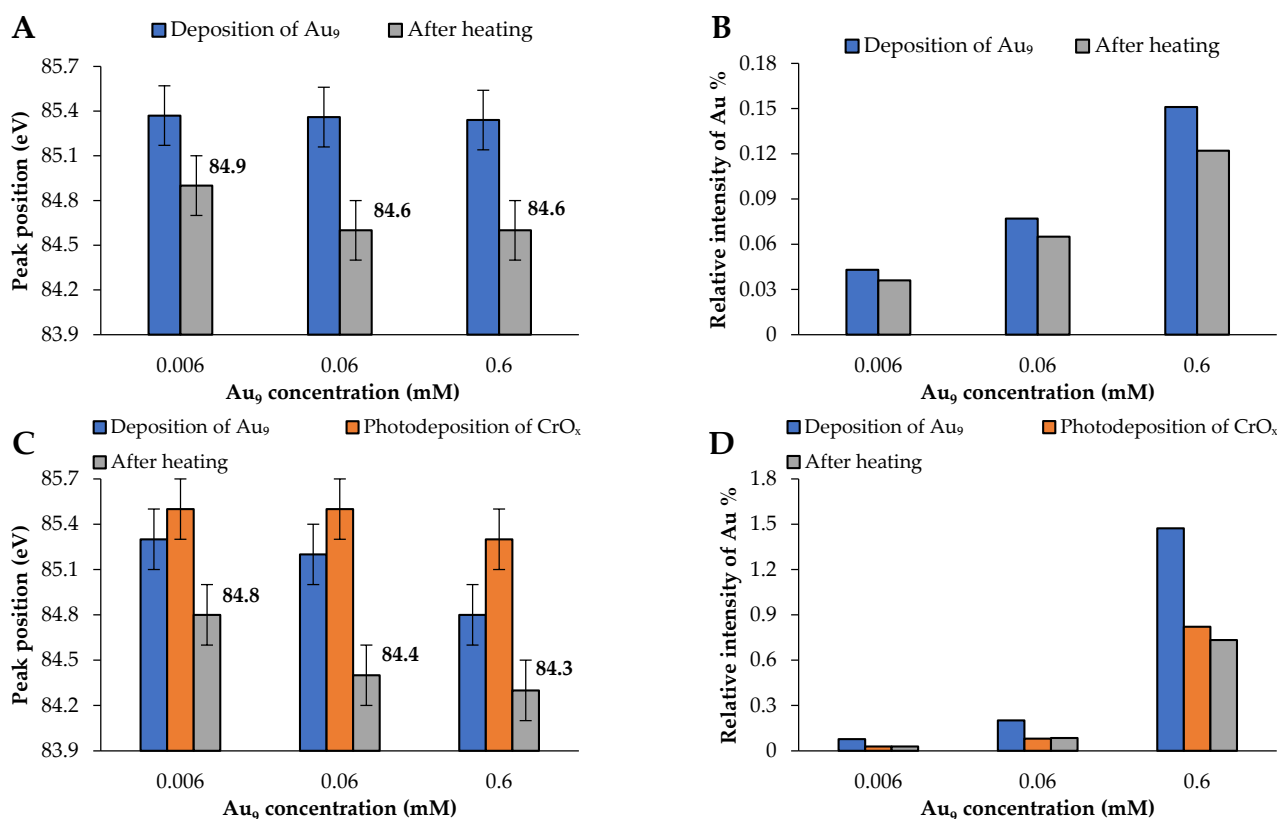
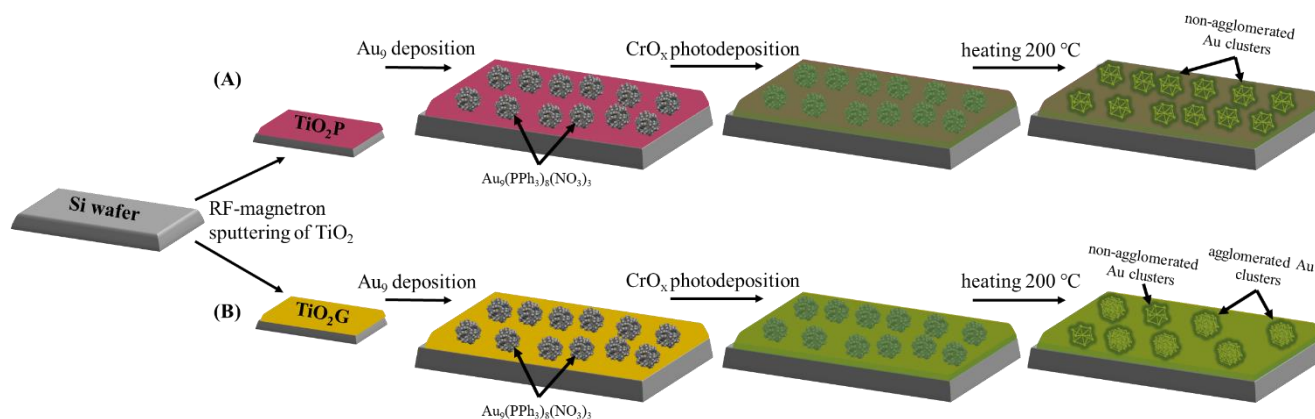


Figure 5. XPS results of Au₉ deposited on TiO₂G for three different Au₉ concentrations: (A) position of Au 4f_{7/2} and (B) relative intensity of Au before and after heating. TiO₂G-Au₉ with the CrO_x layer: (C) position of Au 4f_{7/2} and (D) relative intensity of Au before and after photodeposition of the CrO_x layer and after heating. Note that the vertical scales of (B,D) are different and that the samples in (A,C) are different but are prepared in the same manner.

3.6. XPS of TiO₂P Sample

Without the CrO_x layer and before heating, the Au 4f_{7/2} peaks appeared at 85.1–85.4 eV with an FWHM of 1.7–1.8 eV (Figure 4A), whereas after heating, the Au 4f_{7/2} peaks shifted to slightly lower binding energies (84.7–84.8 eV) and FWHM (1.5–1.6 eV), and also showed a decrease in relative Au intensity across all Au₉ concentrations (Figure 4B). The results of the samples covered with a CrO_x layer are shown in Figure 4C,D. The Au 4f_{7/2} peak positions of TiO₂P-Au₉ after CrO_x deposition but before heating were observed at 85.3 eV and an FWHM of 1.6 eV for all three concentrations. Note that the Au relative intensities decrease after the photodeposition of the CrO_x layer, confirming the coverage of Au clusters with the CrO_x layer (Figure 4D). After heating, the XPS peak position decreases slightly to 85.0 eV with no significant change in FWHM. The relative Au intensities also remained unchanged upon heating. XPS has been shown previously to be a reliable indicator of the size of phosphine-protected Au₉ clusters through the final state effect [21,28,31–36]. Generally, non-agglomerated Au₉ clusters on TiO₂ appear at a high binding peak (HBP) between 85.0–85.4 eV with an FWHM of 1.7 ± 0.2 eV, and agglomerated Au₉ clusters shift toward a low binding peak (LBP) at 84 eV with a decreasing FWHM that corresponds to bulk Au [28,31–35]. This XPS interpretation has been confirmed by correlating the XPS results with other techniques, such as HRTEM [33,34]. Here, the Au 4f_{7/2} peak positions of TiO₂P-Au₉ without the CrO_x layer after heating indicate a small degree of agglomeration of the Au₉ clusters for all concentrations. This is further confirmed by a small decrease in Au intensity after heating, indicating that some of the gold is attenuated due to some larger, agglomerated particles. Electrons emitted from the part of the clusters facing toward the substrate are attenuated when leaving the sample, which decreases the overall Au intensity [31,32]. Therefore, the same total amount of gold

deposited on the surface will have a lower intensity for large gold particles than that of small gold clusters. In contrast to the CrO_x layer of the Au $4f_{7/2}$ peaks, positions are unchanged after heating and there is no further decrease in the Au relative intensities, indicating that Au clusters remain non-agglomerated clusters with CrO_x coverage (see Scheme 1A). It is important to note that there is a decrease in Au intensity after photodeposition of the CrO_x layer due to the coverage of Au_9 clusters (Figure 4D). These results are in agreement with our previous report showing that CrO_x overlayers inhibit the agglomeration of Au clusters [28].



Scheme 1. Schematic illustration of the experimental procedure for preparing (A) $\text{TiO}_2\text{P-Au}_9\text{-CrO}_x$ and (B) $\text{TiO}_2\text{G-Au}_9\text{-CrO}_x$.

The P 2p spectra of $\text{TiO}_2\text{P-Au}_9$ without and with the CrO_x layer before and after heating are shown in Figure S8 and the peak positions are discussed in the Supplementary Section. The Cr 2p spectra for $\text{TiO}_2\text{P-Au}_9\text{-CrO}_x$ before and after heating at the three different concentrations are shown in Figure S9. A summary of all the Cr 2p_{3/2} peak positions is shown in Table S3 and the peak positions are discussed in the Supplementary Section.

3.7. XPS of TiO_2G Sample

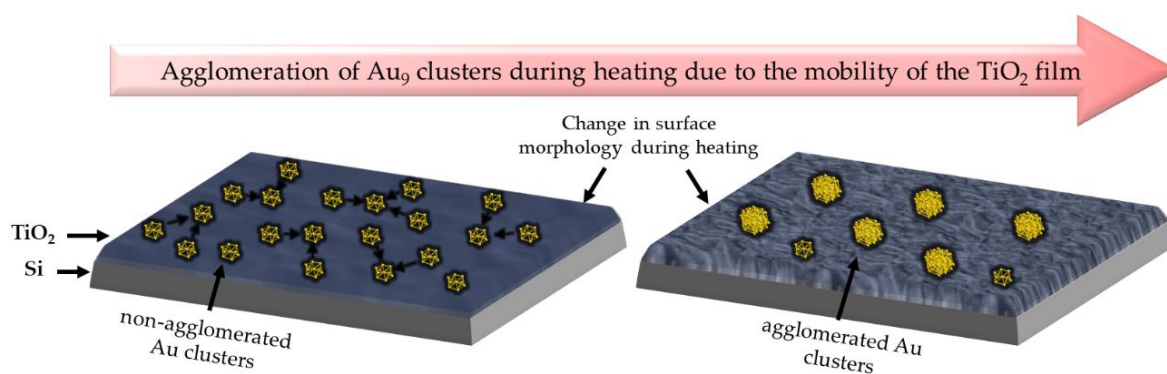
For the thicker film, $\text{TiO}_2\text{G-Au}_9$, the Au $4f_{7/2}$ peak positions before heating for all three different concentrations appeared at the HBP at 85.3 ± 0.1 eV (Figure 5A) and an FWHM of 1.8 ± 0.2 eV, corresponding to non-agglomerated Au clusters. However, after heating, the Au $4f_{7/2}$ shifted toward lower energy (84.6–84.9 eV) and an FWHM of 1.5–1.7 eV with a decrease in Au intensity (Figure 5B), indicating that Au clusters are partially agglomerated. With the CrO_x layer deposited before heating, the Au $4f_{7/2}$ peak positions are observed at the HBP position at 85.3–85.5 eV (Figure 5C), with a decrease in Au $4f_{7/2}$ intensity due to the coverage of the CrO_x layer on Au_9 clusters (Figure 5D). There is a slight increase in the binding energy of the Au 4f peak after the photodeposition of CrO_x , and we do not know if this is a significant change or not. However, the position found can be used as an indication of the presence of non-agglomerated Au clusters. With the CrO_x layer after heating, the Au $4f_{7/2}$ peak positions have further shifted to lower energy (84.3–84.8 eV) positions and an FWHM of 1.3–1.8 eV with a decrease in Au intensity, which is attributed to further agglomeration of the Au clusters based on the final state effect (see Scheme 1B). The degree of agglomeration increases with increasing Au_9 concentration for both cases (without and with the CrO_x layer). Note here the difference; Au clusters on the surface of TiO_2G undergo increased agglomeration after heating, even in the presence of the CrO_x layer. This is different to the TiO_2P , where Au clusters are less likely to agglomerate under the CrO_x layer after heating. This difference will be further discussed below.

The chemical state of the phosphorous ligands of $\text{TiO}_2\text{G-Au}_9$ without and with the CrO_x layer, both before and after heating, was determined using the P 2p region (see Figure S10 for more information and accompanying text). Figure S11 shows the Cr 2p spectra for $\text{TiO}_2\text{G-Au}_9\text{-CrO}_x$ before and after heating of the three different concentrations. All the Cr

$2p_{3/2}$ peak positions are given in Table S4 and the peak positions are discussed in the Supplementary Section.

3.8. Effect of the TiO_2 Film Thickness

The protective effect of the CrO_x layer on the agglomeration of Au_9 clusters is not the same for both the TiO_2P and TiO_2G substrates. The agglomeration of Au_9 clusters is inhibited on TiO_2P with the CrO_x overlayer but not on TiO_2G , which shows a higher degree of agglomeration. The coverage of the CrO_x layer on Au_9 clusters for both substrates is demonstrated by the decrease in the Au-XPS intensities. After heating, it is observed that the relative amount of CrO_x decreases for both films (Table S5). Our previous studies on a similar system revealed that the CrO_x layer diffuses into a TiO_2 film after heating to 600 °C due to the differences in surface energy between TiO_2 and CrO_x [26]. In this study, both films were heated to only 200 °C, however, CrO_x on TiO_2G experienced more diffusion of CrO_x into the film compared to TiO_2P . One possibility for the higher degree of Au_9 agglomeration and CrO_x diffusion is the mobility of the TiO_2 film. Cluster agglomeration can be due to either (i) growth of the clusters over the surface or (ii) mobility of the substrate. In the case of (i), the cluster growth and agglomeration on a substrate can be ascribed to either Smoluchowski ripening or Ostwald ripening mechanisms. For Smoluchowski ripening, the agglomeration of clusters is caused by the collision and coalescence of entire clusters to larger particles [37]. For Ostwald ripening, the growth of larger particles takes place by the detachment of single atoms, which diffuse onto a nearby cluster or nanoparticle [38]. In the case of (ii), a section of the substrate to which a cluster is adsorbed moves closer to another section of the substrate, which has another adsorbed cluster. The significant change in the surface morphology of TiO_2G after heating (Ra: 11.7 nm and Rq: 13.4 nm) compared to TiO_2P (Ra: 0.4 nm and Rq: 0.5 nm) strongly suggests that the agglomeration of the Au_9 clusters with different concentrations on TiO_2G after heating is due to the high distortion of the surface upon heating. A higher mobility of the TiO_2 substrate during heating means that the local surface beneath an Au cluster moves larger distances compared to a substrate which exhibits lower mobility during heating (see Scheme 2). The high mobility of the thick film is assumed to be due to the recrystallisation during heating, which is in agreement with previous studies [17,19,30]. With increasing mobility, the likelihood of close contact between two or more Au clusters increases, and thus the likelihood of agglomeration is also increased. Furthermore, the degree of agglomeration of the Au clusters is larger for the thicker TiO_2G substrate compared to the thinner TiO_2P substrate.



Scheme 2. Schematic illustration showing the agglomeration mechanism of Au_9 clusters on the TiO_2G film during heating.

4. Conclusions

In summary, the change in surface morphology of two different film thicknesses of RF sputter-deposited TiO_2 (~400 nm and ~1100 nm) was examined and compared upon heating. After heating, the thick TiO_2 film showed a larger change in surface morphology, which is associated with higher mobility during heating compared to the thin TiO_2 film. The difference in mobility is attributed to the differences in the total amount of amorphous

TiO₂ transformed to anatase in each of the films, which then results in differences in the morphology of the surface upon heating. Au₉ clusters were used as a probe for TiO₂ mobility. Au₉ clusters were deposited onto the two different TiO₂ films, followed by photodeposition of the CrO_x layer. After heating, the Au clusters on the thicker film showed a larger degree of agglomeration compared to the thinner film. The higher mobility of the thick film during heating increased the probability of close encounters of Au clusters, which resulted in agglomeration of the Au₉ clusters even in the presence of a CrO_x overlayer. In contrast, the lower mobility of the thin film resulted in less agglomeration of the Au₉ clusters after heating.

Supplementary Materials: The following supporting information can be downloaded at: <https://www.mdpi.com/article/10.3390/nano12183218/s1>. The supporting information shows the EDAX-SEM elemental mapping of the TiO₂P and TiO₂G cross-section images, the details of the XP spectra, their fitting, and quantification. Figure S1: A photo of the TiO₂P (left) and TiO₂G (right) films. Figure S2: UV-Vis spectrum of Au₉(PPh₃)₈(NO₃)₃ in Methanol. Figure S3: Cross-section SEM-EDAX elemental maps of Ti, O and Si of TiO₂P and TiO₂G. Note that the scale bars are different. Figure S4: 3D Profile of (A) TiO₂P before heating, (B) TiO₂P after heating, (C) before heating, TiO₂G and (D) TiO₂G after heating (area 16 × 16 μm). Figure S5: Surface morphology with the average of Ra and Rq values of (A) TiO₂P before heating, (B) TiO₂P after heating, (C) before heating, TiO₂G and (D) TiO₂G after heating. (area 595 × 595 μm). It is important to know that the scale bars are different. Figure S6: XP spectra of Au 4f of (A) TiO₂P-Au₉: after Au₉ deposition (blue) and after heating (grey) (B) TiO₂P-Au₉-CrO_x: after Au₉ deposition (blue), after CrO_x layer photodeposited (orange) and after heating (grey). Figure S7: XP spectra of Au 4f of (A) TiO₂G-Au₉: after Au₉ deposition (blue) and after heating (grey) (B) TiO₂G-Au₉-CrO_x: after Au₉ deposition (blue), after CrO_x layer photodeposited (orange) and after heating (grey). Figure S8: XP spectra of P 2p of (A) TiO₂P-Au₉: after Au₉ deposition (blue) and after heating (grey) (B) TiO₂P-Au₉-CrO_x: after Au₉ deposition (blue), after CrO_x layer photodeposited (orange), and after heating (grey). Figure S9: XP spectra of Cr 2p of the TiO₂P-Au₉-CrO_x sample of (A) 0.006mM sample, (B) 0.06mM sample and (C) 0.6mM sample: after CrO_x layer photodeposited (orange) and after heating (grey). Figure S10: XP spectra of P 2p of (A) TiO₂G-Au₉: after Au₉ deposition (blue) and after heating (grey) (B) TiO₂G-Au₉-CrO_x: after Au₉ deposition (blue), after CrO_x layer photodeposited (orange), and after heating (grey). Figure S11: XP spectra of Cr 2p of the TiO₂G-Au₉-CrO_x sample of (A) 0.006mM sample, (B) 0.06mM sample and (C) 0.6mM sample: after CrO_x layer photodeposited (orange) and after heating (grey). Table S1: XPS Au 4f_{7/2} peak positions and FWHM of TiO₂P-Au₉ and TiO₂P-Au₉-CrO_x. Table S2: XPS Au 4f_{7/2} peak positions and FWHM of TiO₂G-Au₉ and TiO₂G-Au₉-CrO_x. Table S3: XPS Cr 2p_{3/2} peak positions and FWHM of TiO₂P-Au₉-CrO_x. Table S4: XPS Cr 2p_{3/2} peak positions and FWHM of TiO₂G-Au₉-CrO_x. Table S5: XPS relative amount of Cr 2p_{3/2} to Ti 2p_{3/2} of TiO₂P-Au₉-CrO_x and TiO₂G-Au₉-CrO_x. References [39–44] are cited in the supplementary materials.

Author Contributions: Conceptualization, A.S.A., G.F.M. and G.G.A.; Data curation, A.S.A. and G.G.A.; Formal analysis, A.S.A., Y.Y. and A.R.; Funding acquisition, G.F.M. and G.G.A.; Investigation, A.S.A., Y.Y. and A.R.; Methodology, A.S.A., G.F.M. and G.G.A.; Resources, S.T. and G.G.A.; Supervision, G.G.A.; Visualization, A.S.A.; Writing—original draft, A.S.A.; Writing—review & editing, A.S.A., Y.Y., A.R., S.T., G.F.M. and G.G.A. All authors have read and agreed to the published version of the manuscript.

Funding: Australian Synchrotron, Victoria, Australia (AS1/SXR/15819); US Army project FA5209-16-R-0017; Australian Solar Thermal Research Institute (ASTRI), a project supported by the Australian Government, through the Australian Renewable Energy Agency (ARENA).

Institutional Review Board Statement: Not applicable.

Informed Consent Statement: Not applicable.

Data Availability Statement: The data that support the findings of this study are available from the corresponding author upon reasonable request.

Acknowledgments: Part of this research was undertaken on the soft X-ray spectroscopy beamline at the Australian Synchrotron, Victoria, Australia (AS1/SXR/15819). The work was supported by the US Army project FA5209-16-R-0017. This research was performed as part of the Australian Solar Thermal Research Institute (ASTRI), a project supported by the Australian Government, through the Australian Renewable Energy Agency (ARENA). We would like to thank Dr Bruce Cowie from the Australian Synchrotron for his assistance. The authors acknowledge the facilities, and the scientific and technical assistance, of Microscopy Australia (formerly known as AMMRF) and the Australian National Fabrication Facility (ANFF) at Flinders University. The authors acknowledge Flinders Microscopy and Microanalysis and their expertise. The authors thank A/Prof Vladimir Golovko (Canterbury University) for providing access to the Au₉(PPh₃)₈(NO₃)₃ clusters. The authors acknowledge Dr Benjamin Wade at Adelaide Microscopy (University of Adelaide).

Conflicts of Interest: The authors declare no conflict of interest.

References

1. Daghrir, R.; Drogui, P.; Robert, D. Modified TiO₂ For Environmental Photocatalytic Applications: A Review. *Ind. Eng. Chem. Res.* **2013**, *52*, 3581–3599. [[CrossRef](#)]
2. Linsebigler, A.L.; Lu, G.; Yates, J.T. Photocatalysis on TiO₂ Surfaces: Principles, Mechanisms, and Selected Results. *Chem. Rev.* **1995**, *95*, 735–758. [[CrossRef](#)]
3. Brinker, C.J.; Harrington, M.S. Sol-gel Derived Antireflective Coatings for Silicon. *Sol. Energy Mater.* **1981**, *5*, 159–172. [[CrossRef](#)]
4. Lottiaux, M.; Boulesteix, C.; Nihoul, G.; Varnier, F.; Flory, F.; Galindo, R.; Pelletier, E. Morphology and Structure of TiO₂ Thin Layers vs. Thickness and Substrate Temperature. *Thin Solid Film.* **1989**, *170*, 107–126. [[CrossRef](#)]
5. Yeung, K.S.; Lam, Y.W. A Simple Chemical Vapour Deposition Method for Depositing Thin TiO₂ Films. *Thin Solid Film.* **1983**, *109*, 169–178. [[CrossRef](#)]
6. Aarik, J.; Aidla, A.; Uustare, T.; Kukli, K.; Sammelselg, V.; Ritala, M.; Leskelä, M. Atomic Layer Deposition of TiO₂ Thin Films from TiI₄ and H₂O. *Appl. Surf. Sci.* **2002**, *193*, 277–286. [[CrossRef](#)]
7. Dakka, A.; Lafait, J.; Abd-Lefdil, M.; Sella, C. Optical Study of Titanium Dioxide Thin Films Prepared by RF Sputtering. *Moroc. J. Condens. Matter* **1999**, *2*, 153–156.
8. Tanemura, S.; Miao, L.; Wunderlich, W.; Tanemura, M.; Mori, Y.; Toh, S.; Kaneko, K. Fabrication and Characterization of Anatase/Rutile-TiO₂ Thin Films by Magnetron Sputtering: A Review. *Sci. Technol. Adv. Mater.* **2005**, *6*, 11–17. [[CrossRef](#)]
9. Miao, L.; Jin, P.; Kaneko, K.; Terai, A.; Nabatova-Gabain, N.; Tanemura, S. Preparation and characterization of polycrystalline anatase and rutile TiO₂ thin films by rf magnetron sputtering. *Appl. Surf. Sci.* **2003**, *212–213*, 255–263. [[CrossRef](#)]
10. Wang, T.M.; Zheng, S.K.; Hao, W.C.; Wang, C. Studies on photocatalytic activity and transmittance spectra of TiO₂ thin films prepared by r.f. magnetron sputtering method. *Surf. Coat. Technol.* **2002**, *155*, 141–145. [[CrossRef](#)]
11. Ye, Q.; Liu, P.Y.; Tang, Z.F.; Zhai, L. Hydrophilic properties of nano-TiO₂ thin films deposited by RF magnetron sputtering. *Vacuum* **2007**, *81*, 627–631. [[CrossRef](#)]
12. Huang, C.H.; Tsao, C.C.; Hsu, C.Y. Study on the photocatalytic activities of TiO₂ films prepared by reactive RF sputtering. *Ceram. Int.* **2011**, *37*, 2781–2788. [[CrossRef](#)]
13. Yoo, D.; Kim, I.; Kim, S.; Hahn, C.H.; Lee, C.; Cho, S. Effects of annealing temperature and method on structural and optical properties of TiO₂ films prepared by RF magnetron sputtering at room temperature. *Appl. Surf. Sci.* **2007**, *253*, 3888–3892. [[CrossRef](#)]
14. Hou, Y.-Q.; Zhuang, D.-M.; Zhang, G.; Zhao, M.; Wu, M.-S. Influence of annealing temperature on the properties of titanium oxide thin film. *Appl. Surf. Sci.* **2003**, *218*, 98–106. [[CrossRef](#)]
15. Grilli, M.L.; Yilmaz, M.; Aydogan, S.; Cirak, B.B. Room temperature deposition of XRD-amorphous TiO₂ thin films: Investigation of device performance as a function of temperature. *Ceram. Int.* **2018**, *44*, 11582–11590. [[CrossRef](#)]
16. Mathews, N.R.; Morales, E.R.; Cortés-Jacome, M.A.; Toledo Antonio, J.A. TiO₂ Thin Films—Influence of Annealing Temperature on Structural, Optical and Photocatalytic Properties. *Sol. Energy* **2009**, *83*, 1499–1508. [[CrossRef](#)]
17. Meng, F.; Xiao, L.; Sun, Z. Thermo-induced hydrophilicity of nano-TiO₂ thin films prepared by RF magnetron sputtering. *J. Alloy. Compd.* **2009**, *485*, 848–852. [[CrossRef](#)]
18. Taherniya, A.; Raoufi, D. Thickness dependence of structural, optical and morphological properties of sol-gel derived TiO₂ thin film. *Mater. Res. Express* **2018**, *6*, 016417. [[CrossRef](#)]
19. Çörekçi, Ş.; Kizilkaya, K.; Asar, T.; Öztürk, M.; Çakmak, M.; Ozelik, S. Effects of Thermal Annealing and Film Thickness on the Structural and Morphological Properties of Titanium Dioxide Films. *Acta Phys. Pol. A* **2012**, *121*, 247–248. [[CrossRef](#)]
20. Pichugina, D.A.; Kuz'menko, N.E.; Shestakov, A.F. Ligand-protected gold clusters: The structure, synthesis and applications. *Russ. Chem. Rev.* **2015**, *84*, 1114–1144. [[CrossRef](#)]
21. Adnan, R.H.; Madrideo, J.M.L.; Alotabi, A.S.; Metha, G.F.; Andersson, G.G. A Review of State of the Art in Phosphine Ligated Gold Clusters and Application in Catalysis. *Adv. Sci.* **2022**, *2022*, 2105692. [[CrossRef](#)] [[PubMed](#)]
22. Daughtry, J.; Alotabi, A.S.; Howard-Fabretto, L.; Andersson, G.G. Composition and Properties of RF-Sputter Deposited Titanium Dioxide Thin Films. *Nanoscale Adv.* **2021**, *3*, 1077–1086. [[CrossRef](#)]

23. Yuan, X.; Ye, Y.; Lian, M.; Wei, Q. Structural Coloration of Polyester Fabrics Coated with Al/TiO₂ Composite Films and Their Anti-Ultraviolet Properties. *Materials* **2018**, *11*, 1011. [[CrossRef](#)] [[PubMed](#)]
24. Diamanti, M.V.; Del Curto, B.; Pedefferri, M. Interference Colors of Thin Oxide Layers on Titanium. *Color Res. Appl.* **2008**, *33*, 221–228. [[CrossRef](#)]
25. Wen, F.; Englert, U.; Gutrath, B.; Simon, U. Crystal Structure, Electrochemical and Optical Properties of [Au₉(PPh₃)₈](NO₃)₃. *Eur. J. Inorg. Chem.* **2008**, *2008*, 106–111. [[CrossRef](#)]
26. Alotabi, A.S.; Gibson, C.T.; Metha, G.F.; Andersson, G.G. Investigation of the Diffusion of Cr₂O₃ into Different Phases of TiO₂ upon Annealing. *ACS Appl. Energy Mater.* **2021**, *4*, 322–330. [[CrossRef](#)]
27. Acres, R.G.; Ellis, A.V.; Alvino, J.; Lenahan, C.E.; Khodakov, D.A.; Metha, G.F.; Andersson, G.G. Molecular Structure of 3-Aminopropyltriethoxysilane Layers Formed on Silanol-Terminated Silicon Surfaces. *J. Phys. Chem. C* **2012**, *116*, 6289–6297. [[CrossRef](#)]
28. Alotabi, A.S.; Yin, Y.; Redaa, A.; Tesana, S.; Metha, G.F.; Andersson, G.G. Cr₂O₃ layer inhibits agglomeration of phosphine-protected Au₉ clusters on TiO₂ films. *J. Chem. Phys.* **2021**, *155*, 164702. [[CrossRef](#)]
29. Ali, S.; Granbohm, H.; Lahtinen, J.; Hannula, S.-P. Titania Nanotubes Prepared by Rapid Breakdown Anodization for Photocatalytic Decolorization of Organic Dyes under UV and Natural Solar Light. *Nanoscale Res. Lett.* **2018**, *13*, 179. [[CrossRef](#)]
30. Chandra Sekhar, M.; Kondaiah, P.; Jagadeesh Chandra, S.V.; Mohan Rao, G.; Uthanna, S. Substrate temperature influenced physical properties of silicon MOS devices with TiO₂ gate dielectric. *Surf. Interface Anal.* **2012**, *44*, 1299–1304. [[CrossRef](#)]
31. Anderson, D.P.; Alvino, J.F.; Gentleman, A.; Al Qahtani, H.; Thomsen, L.; Polson, M.I.; Metha, G.F.; Golovko, V.B.; Andersson, G.G. Chemically-Synthesised, Atomically-Precise Gold Clusters Deposited and Activated on Titania. *Phys. Chem. Chem. Phys.* **2013**, *15*, 3917–3929. [[CrossRef](#)] [[PubMed](#)]
32. Anderson, D.P.; Adnan, R.H.; Alvino, J.F.; Shipper, O.; Donoeva, B.; Ruzicka, J.-Y.; Al Qahtani, H.; Harris, H.H.; Cowie, B.; Aitken, J.B. Chemically Synthesised Atomically Precise Gold Clusters Deposited and Activated on Titania. Part II. *Phys. Chem. Chem. Phys.* **2013**, *15*, 14806–14813. [[CrossRef](#)] [[PubMed](#)]
33. Al Qahtani, H.S.; Kimoto, K.; Bennett, T.; Alvino, J.F.; Andersson, G.G.; Metha, G.F.; Golovko, V.B.; Sasaki, T.; Nakayama, T. Atomically resolved structure of ligand-protected Au₉ clusters on TiO₂ nanosheets using aberration-corrected STEM. *J. Chem. Phys.* **2016**, *144*, 114703. [[CrossRef](#)] [[PubMed](#)]
34. Al Qahtani, H.S.; Metha, G.F.; Walsh, R.B.; Golovko, V.B.; Andersson, G.G.; Nakayama, T. Aggregation Behavior of Ligand-Protected Au₉ Clusters on Sputtered Atomic Layer Deposition TiO₂. *J. Phys. Chem. C* **2017**, *121*, 10781–10789. [[CrossRef](#)]
35. Howard-Fabretto, L.; Andersson, G.G. Metal Clusters on Semiconductor Surfaces and Application in Catalysis with a Focus on Au and Ru. *Adv. Mater.* **2020**, *32*, 1904122. [[CrossRef](#)] [[PubMed](#)]
36. Alotabi, A.S.; Osborn, D.J.; Ozaki, S.; Kataoka, Y.; Negishi, Y.; Tesana, S.; Metha, G.F.; Andersson, G.G. Suppression of phosphine-protected Au₉ cluster agglomeration on SrTiO₃ particles using a chromium hydroxide layer. *Mater. Adv.* **2022**, *3*, 3620–3630. [[CrossRef](#)]
37. Smoluchowski, M.V. Drei vortrage uber diffusion, brownsche bewegung und koagulation von kolloidteilchen. *Z. Fur Phys.* **1916**, *17*, 557–585.
38. Ostwald, W. Blocking of Ostwald ripening allowing long-term stabilization. *Phys. Chem.* **1901**, *37*, 385.
39. Wilcoxon, J.P.; Provencio, P. Etching and Aging Effects in Nanosize Au Clusters Investigated Using High-Resolution Size-Exclusion Chromatography. *J. Phys. Chem. B* **2003**, *107*, 12949. [[CrossRef](#)]
40. Moulder, J.F. Handbook of X-ray photoelectron spectroscopy: A reference book of standard data for use in x-ray photoelectron spectroscopy. In *Handbook of X-ray Photoelectron Spectroscopy*; Perkin-Elmer Corporation: Waltham, MA, USA, 1992.
41. Biesinger, M.C.; Brown, C.; Mycroft, J.R.; Davidson, R.D.; McIntyre, N.S. X-ray photoelectron spectroscopy studies of chromium compounds. *Surf. Interface Anal.* **2004**, *36*, 1550–1563. [[CrossRef](#)]
42. Kawawaki, T.; Kataoka, Y.; Hirata, M.; Akinaga, Y.; Takahata, R.; Wakamatsu, K.; Fujiki, Y.; Kataoka, M.; Kikkawa, S.; Alotabi, A.S.; et al. Creation of High-Performance Heterogeneous Photocatalysts by Controlling Ligand Desorption and Particle Size of Gold Nanocluster. *Angew. Chem. Int. Ed.* **2021**, *60*, 21340–21350. [[CrossRef](#)] [[PubMed](#)]
43. Madrudejos, J.M.L.; Harada, T.; Falcinella, A.J.; Small, T.D.; Golovko, V.B.; Andersson, G.G.; Metha, G.F.; Kee, T.W. Optical Properties of the Atomically Precise C₄ Core [Au₉(PPh₃)₈]³⁺ Cluster Probed by Transient Absorption Spectroscopy and Time-Dependent Density Functional Theory. *J. Phys. Chem. C* **2021**, *125*, 2033–2044. [[CrossRef](#)]
44. Krishnan, G.; Al Qahtani, H.S.; Li, J.; Yin, Y.; Eom, N.; Golovko, V.B.; Metha, G.F.; Andersson, G.G. Investigation of Ligand-Stabilized Gold Clusters on Defect-Rich Titania. *J. Phys. Chem. C* **2017**, *121*, 28007–28016. [[CrossRef](#)]